

Plasmon-Phonon Hybridization in Doped Semiconductors from First Principles

Jae-Mo Lihm^{✉*} and Cheol-Hwan Park^{✉†}

*Department of Physics and Astronomy, Seoul National University, Seoul 08826, Korea;
Center for Correlated Electron Systems, Institute for Basic Science, Seoul 08826, Korea
and Center for Theoretical Physics, Seoul National University, Seoul 08826, Korea*

 (Received 9 February 2024; accepted 24 July 2024; published 10 September 2024)

Although plasmons and phonons are the collective excitations that govern the low-energy physics of doped semiconductors, their nonadiabatic hybridization and mutual screening have not been studied from first principles. We achieve this goal by transforming the Dyson equation to the frequency-independent dynamical matrix of an equivalent damped oscillator. Calculations on doped GaAs and TiO₂ agree well with available Raman data and await immediate experimental confirmation from infrared, neutron, electron-energy-loss, and angle-resolved photoemission spectroscopies.

DOI: [10.1103/PhysRevLett.133.116402](https://doi.org/10.1103/PhysRevLett.133.116402)

Doped semiconductors play the most essential role in modern electronics. An important property of doped semiconductors is the presence of low-energy collective charge excitations, plasmons. Plasmons in doped semiconductors strongly couple to other low-energy excitations, particularly phonons. This coupling determines the low-energy spectroscopic properties of doped semiconductors. In addition, electron-phonon and electron-plasmon interactions are the two major contributions to electron scattering at room temperature. Therefore, understanding and modeling the interplay of plasmons and phonons and their coupling to electrons is crucial for studying doped semiconductors.

Plasmon-phonon coupling can be divided into three regimes in order of increasing doping: anti-adiabatic, resonant, and adiabatic [1,2]. The change in the plasmon energy relative to the phonon energy governs the crossover from insulators to metals and affects many properties, such as the splitting between longitudinal optical (LO) and transverse optical (TO) phonons and the presence of long-range electric fields (Table I). At low doping, the phonon energy is higher; hence, the plasmons do not screen the phonons, and both the LO-TO splitting and phonon-induced long-range electric fields are present, just as in undoped systems. At intermediate doping, where the plasmon energies are comparable to the phonon energies, the two modes hybridize strongly [3–6]. This hybridization leads to a level anticrossing behavior that was confirmed by Raman experiments on GaAs [7,8]. At even higher doping, the plasmon energy exceeds the LO phonon energy, and the plasmons fully screen the electric field generated by the

phonons. The LO-TO splitting and the electron-phonon coupling are then strongly suppressed.

A major hurdle in studying plasmon-phonon coupling in real materials has been the lack of an efficient first-principles methodology. In the anti-adiabatic and resonant regime, one needs a nonadiabatic description of phonons [9–12] that goes beyond the Born-Oppenheimer approximation. In particular, one needs to capture the full frequency dependence of the dielectric function and the phonon self-energy [13]. Because of the high computational cost of such calculations, few studies considered the nonadiabatic coupling [14–17], relying on simplified models of the electron or phonon dispersion. Previous first-principles studies on doped semiconductors, namely, Refs. [1,18], have neglected any feedback from phonons to plasmons and used the electron gas model to compute the free-carrier screening. References [19,20] represent a different line of work, which treats doping using the static density functional perturbation theory (DFPT) and thus cannot reproduce any nonadiabatic effects. Another important open problem is to understand how the plasmon-phonon modes couple to the electrons. While there have been separate first-principles calculations on the electron-phonon and electron-plasmon couplings [18,21], a unified first-principles theory of the electron-plasmon-phonon coupling has not been developed. Developing a first-principles method for calculating the plasmon-phonon hybridization in all three regimes remains an open challenge in modeling doped semiconductors [13,22].

In this study, we develop a fully first-principles description of the plasmon-phonon hybridization in doped semiconductors. We transform the *nonadiabatic* problem of computing the phonon Green's function into an *adiabatic* problem of diagonalizing a plasmon-phonon dynamical matrix, significantly reducing the computational cost. We first validate our new method by quantitatively reproducing

*Contact author: jaemo.lihm@gmail.com

†Contact author: cheolhwan@snu.ac.kr

TABLE I. Three regimes of plasmon-phonon (pl-ph) hybridization. ω_{pl} and ω_{ph} denote the plasmon and phonon energy scales, respectively. (O*: The LO phonons form a plasmon-phonon hybrid, making the concept of LO-TO splitting unclear.)

Regime	Energies	LO-TO splitting	Long-range electric field
Anti-adiabatic	$\omega_{\text{pl}} \ll \omega_{\text{ph}}$	O	Phonon
Resonant	$\omega_{\text{pl}} \approx \omega_{\text{ph}}$	O*	pl-ph hybrid
Adiabatic	$\omega_{\text{pl}} \gg \omega_{\text{ph}}$	X	Plasmon

without any free parameters the dispersion of plasmon-phonon hybrids in GaAs [8] (Fig. 1). We then study the complicated wave-vector-direction-dependent plasmon-phonon coupling of anatase TiO₂, presenting many predictions that await immediate experimental confirmation by infrared (Fig. 2), neutron scattering [Fig. 3(a)], electron energy loss [Fig. 3(b)], and angle-resolved photoemission (Fig. 4) spectroscopies. Our first-principles method can also be widely used to study polarons, transport, and superconductivity of doped semiconductors.

To model plasmon-phonon hybridization, we first perform a static DFPT calculation of the *undoped* system. We then treat the doping using the rigid-band approximation and incorporate the screening effects in the random phase approximation. The doped carriers induce a phonon self-energy [10,23–25]

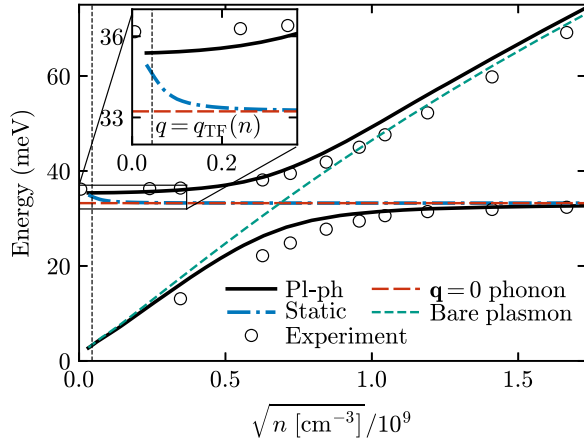


FIG. 1. Doping-dependent energy of the plasmon-phonon (pl-ph) hybrids of n -doped GaAs. The solid black (dash-dotted blue) curves show the result of a nonadiabatic plasmon-phonon (static) calculation. The circles show the experimental measurements of Ref. [8]. The horizontal dashed red line shows the optical phonon energy at $\mathbf{q} = 0$, which corresponds to the TO phonon energy in the case of GaAs. The green dashed line shows the bare plasmon energy. We use the experimental wave vector $q = 8 \times 10^{-4} \text{ \AA}^{-1}$ in the [110] direction. The vertical dotted line denotes the density $n = 2 \times 10^{15} \text{ cm}^{-3}$ where the Thomas-Fermi wave vector q_{TF} is equal to the experimental wave vector. All calculations in this Letter are performed for $T = 300 \text{ K}$.

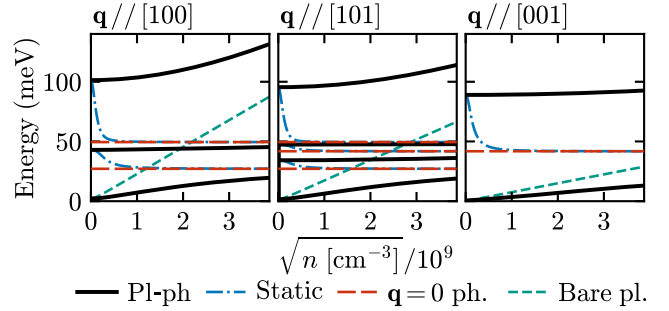


FIG. 2. Doping- and wave-vector-direction-dependent energy of the plasmon-phonon hybrids of n -doped anatase TiO₂ for wave vectors of magnitude $q = 2 \times 10^{-3} \text{ \AA}^{-1}$. Only the hybridized modes are plotted; the other, pure TO or infrared-inactive phonon modes do not hybridize with plasmons.

$$\Pi_{\mu\nu}(\mathbf{q}, \omega) = (g_{\mathbf{q}\mu}^{\text{r}})^* \delta\chi(\mathbf{q}, \omega) g_{\mathbf{q}\nu}^{\text{r}}, \quad (1)$$

where \mathbf{q} is the phonon wave vector, ω the frequency, $\mu, \nu = 1, \dots, N_{\text{ph}}$ the phonon mode indices, $\delta\chi(\mathbf{q}, \omega)$ the interacting susceptibility of the doped carriers Sec. S2 in [26], and $g_{\mathbf{q}\mu}^{\text{r}}$ the long-range electron-phonon vertex Sec. S5 in [26]. This self-energy is nonadiabatic, i.e., frequency dependent, and thus leads to a nontrivial renormalization that gives rise to additional peaks in the phonon spectral function.

When calculating the interacting electronic susceptibility in the random phase approximation, we neglect local field effects, as has been validated for doped semiconductors [19,55]. We model the frequency dependence of the susceptibility using a plasmon-pole model [56]:

$$\delta\chi(\mathbf{q}, \omega) = \frac{1}{U_{\mathbf{q}}} \frac{\Omega_{\mathbf{q}0}^2}{(\omega + i\gamma_{\mathbf{q}0})^2 - \omega_{\mathbf{q}0}^2}, \quad (2)$$

where $U_{\mathbf{q}} = 4\pi e^2 / (Vq^2\epsilon_{\mathbf{q}}^{\infty})$ with $\epsilon_{\mathbf{q}}^{\infty} = \hat{\mathbf{q}} \cdot \epsilon^{\infty} \cdot \hat{\mathbf{q}}$ is the macroscopic Coulomb interaction screened by the electronic dielectric tensor ϵ^{∞} of the undoped system and V the unit cell volume. The model has three parameters, $\Omega_{\mathbf{q}0}$, $\omega_{\mathbf{q}0}$, and $\gamma_{\mathbf{q}0}$: the plasmon strength, frequency, and linewidth. The plasmon linewidth is nonzero in the electron-hole continuum and captures the decay of plasmons into electron-hole pairs. Our method can be straightforwardly generalized to treat more complex frequency dependences using the multipole approach [57] (see Sec. S1.E in [26] for details).

With the bare phonon Green's function

$$D_{\mu\nu}^0(\mathbf{q}, \omega) = \delta_{\mu\nu} \frac{1}{(\omega + i0^+)^2 - \omega_{\mathbf{q}\nu}^2}, \quad (3)$$

where $\omega_{\mathbf{q}\nu}$ is the phonon frequency of the undoped system, the full Green's function D is computed by solving the Dyson equation

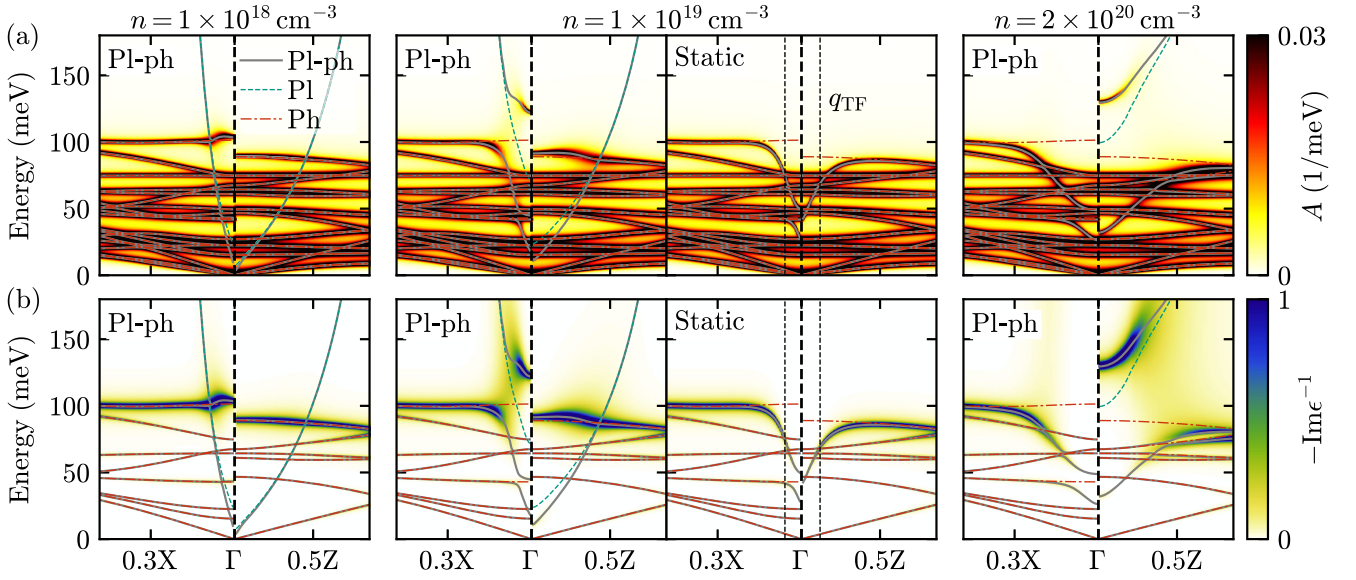


FIG. 3. (a) Phonon spectral function and (b) inverse dielectric function of n -doped anatase TiO_2 . We add an artificial broadening of 0.5 meV to the bare phonon Green's functions for visualization. The third column shows the results obtained with the static approximation, while the others show the results of nonadiabatic plasmon-phonon calculations. The dotted vertical lines in the third column denote the Thomas-Fermi wave vector, the wave vector where the static dielectric function equals twice ϵ_q^∞ . In (b), we plot only the modes contributing to the dielectric function.

$$D_{\mu\nu}^{-1}(\mathbf{q}, \omega) = (D^0)_{\mu\nu}^{-1}(\mathbf{q}, \omega) - \Pi_{\mu\nu}(\mathbf{q}, \omega). \quad (4)$$

Solving Eq. (4) at each ω inflates the computational cost, making this calculation unsuitable for a first-principles application dealing with a large number of wave vectors or materials with a complex unit cell.

Remarkably, it was found that one can exactly transform the problem of solving a *frequency-dependent* fermionic Dyson equation into a simpler problem of diagonalizing a *frequency-independent* matrix by writing the self-energy as a sum over poles, in the context of dynamical mean-field theory [58] and *GW* [59] calculations. In a different context, *semiclassical* studies of phonon-polaritons [60] and spin-lattice coupling [61] have developed dynamical matrices that describe the hybridization of phonons with other bosonic modes. We combine these fascinating ideas and apply them to bosonic plasmon-phonon hybridization, thereby developing a method of solving the phonon Dyson equation via a frequency-independent, $(N_{\text{ph}} + 1)$ -dimensional plasmon-phonon dynamical matrix. In addition, we find that one can incorporate finite bosonic linewidths, which are essential for our study, by diagonalizing a $2(N_{\text{ph}} + 1)$ -dimensional dynamical matrix for a damped oscillator.

If the plasmon linewidth is zero ($\gamma_{q0} = 0^+$), the phonon Green's function has $N_{\text{ph}} + 1$ poles whose energy is the square root of the eigenvalues of an $(N_{\text{ph}} + 1)$ -dimensional plasmon-phonon dynamical matrix

$$\tilde{C}_{\mathbf{q}} = \begin{pmatrix} \omega_{q0}^2 & c_{q1} & c_{q2} & \cdots \\ c_{q1}^* & \omega_{q1}^2 & 0 & \cdots \\ c_{q2}^* & 0 & \omega_{q2}^2 & \cdots \\ \vdots & \vdots & \vdots & \ddots \end{pmatrix}, \quad (5)$$

where the plasmon and phonon frequencies are on the diagonals and the plasmon-phonon coupling amplitudes

$$c_{q\nu} = \Omega_{q0} g_{q\nu}^{\text{lr}} / \sqrt{U_{\mathbf{q}}} \quad (6)$$

on the wings. We denote objects in the $(N_{\text{ph}} + 1)$ -dimensional plasmon-phonon basis by a tilde. They have indices $\alpha = 0, \dots, N_{\text{ph}}$, where 0 corresponds to the plasmon, and the others to the phonons.

We diagonalize $\tilde{C}_{\mathbf{q}}$ with orthonormal eigenvectors as

$$\sum_{\alpha'=0}^{N_{\text{ph}}} \tilde{C}_{\mathbf{q}\alpha\alpha'} \tilde{V}'_{\mathbf{q}\alpha'\beta} = \tilde{\omega}_{\mathbf{q}\beta}^2 \tilde{V}'_{\mathbf{q}\alpha\beta}. \quad (7)$$

The eigenvalue $\tilde{\omega}_{\mathbf{q}\beta}$ is the energy of a plasmon-phonon hybrid mode, and the eigenvector $\tilde{V}'_{\mathbf{q}\alpha\beta}$ encodes the weight of the plasmon ($\alpha = 0$) and phonons ($\alpha = 1, \dots, N_{\text{ph}}$) of the hybrid mode. The phonon Green's function can be written as a sum over these hybrid modes:

$$D_{\mu\nu}(\mathbf{q}, \omega) = \sum_{\beta=0}^{N_{\text{ph}}} \frac{\tilde{V}'_{\mathbf{q}\mu\beta} \tilde{V}'_{\mathbf{q}\nu\beta*}}{(\omega + i0^+)^2 - \tilde{\omega}_{\mathbf{q}\beta}^2}. \quad (8)$$

The dielectric function can be calculated similarly Sec. S81 in [26].

One can derive analogous results for nonzero plasmon linewidth $\gamma_{\mathbf{q}0} \neq 0$ by solving a damped oscillator problem, whose dynamical matrix in the generalized position-velocity coordinate basis is given by

$$\begin{pmatrix} -i\tilde{\Gamma}_{\mathbf{q}} & \mathbb{1} \\ \tilde{C}_{\mathbf{q}} & -i\tilde{\Gamma}_{\mathbf{q}} \end{pmatrix}, \quad (9)$$

where $\tilde{\Gamma}_{\mathbf{q}\alpha\alpha'} = \delta_{\alpha\alpha'}\gamma_{\mathbf{q}\alpha}$ and $\mathbb{1}$ is an $(N_{\text{ph}} + 1)$ -dimensional identity matrix. Now, the plasmon-phonon hybrids have complex eigenvalues whose real and imaginary parts correspond to the energy and linewidth of the hybrid mode, respectively. See Sec. S1 for the details of the derivation of Eqs. (5)–(9) [26].

We first apply our plasmon-phonon method to GaAs, a prototypical material for studying plasmon-phonon hybridization [7,8]. Figure 1 shows the calculated doping dependence of the plasmon-phonon hybrid energies at 300 K, compared to the measured Raman data [8]. We find good quantitative agreement between the experiment and theory without any free parameters. The static approximation completely fails to capture the plasmon-phonon hybridization, leading to a vanishing LO-TO splitting at $n > 2 \times 10^{15} \text{ cm}^{-3}$, the density over which the Thomas-Fermi wave vector exceeds the experimental momentum transfer. Moreover, for an infinitesimal q , the static approximation gives vanishing LO-TO splitting at all doping levels, while the dispersion obtained from the nonadiabatic calculation remains invariant.

We now study plasmon-phonon coupling in anatase TiO_2 . Anatase is a stable, naturally abundant, and nontoxic material widely used in photocatalytic, photovoltaic, and electronic applications [62–67]. Because of its highly tunable electron doping, which is achievable up to $3.5 \times 10^{20} \text{ cm}^{-3}$ [68], and strong electron-phonon coupling, TiO_2 has been a test bed for studying electron-phonon coupling in doped semiconductors, both experimentally [68–70] and theoretically [1,16,18].

Figure 2 shows the energies of the plasmon-phonon hybrids for wave vectors with infinitesimal magnitudes at 300 K. Because of the tetragonal lattice structure with a D_{4h} point group symmetry, one to three phonon modes couple to the plasmons, depending on the direction of the wave vector. The remaining, purely TO or infrared-inactive phonons do not couple to the plasmons; hence, their energies are doping independent. The rich doping dependence and anisotropy of the hybrid modes can be confirmed by infrared spectroscopy.

Figure 3 shows the doping-dependent phonon spectral function and the imaginary part of the inverse dielectric function, which can be measured by neutron scattering and electron energy loss spectroscopies, respectively. Because of the highly anisotropic effective mass, the plasmon energy is anisotropic and discontinuous at $\mathbf{q} = \Gamma$ [71]. Our first-principles calculations fully reveal the anisotropic doping dependence of the plasmon-phonon hybridization. At low doping ($n = 1 \times 10^{18} \text{ cm}^{-3}$), the in-plane and out-of-plane plasma frequencies are both below the corresponding LO frequencies, and TiO_2 is in the anti-adiabatic regime. At $n = 1 \times 10^{19} \text{ cm}^{-3}$, the in-plane LO phonons and plasmons are resonant, while the out-of-plane LO phonon is still in the anti-adiabatic regime. At $n = 2 \times 10^{20} \text{ cm}^{-3}$, the in-plane LO phonons are fully screened and are in the adiabatic regime with vanishing LO-TO splitting, while the out-of-plane phonons are in the resonant regime. This behavior is also reflected in the inverse dielectric function, where the signal is strongest for the LO phonon, hybrid modes, and plasmons in the anti-adiabatic, resonant, and adiabatic regimes, respectively. Moreover, we find a momentum-direction- and momentum-magnitude-dependent anticrossing between plasmons and phonons, as their bare energies approximately scale as q^2 and q^0 , respectively.

Nonadiabaticity is crucial for the description of phonons in the anti-adiabatic and resonant regimes. Unlike the results from the nonadiabatic calculations, static screening yields adiabatic phonons with vanishing LO-TO splitting, continuous spectral functions, and no plasmon-phonon hybridization. It also overly screens the phonons and underestimates the inverse dielectric functions, especially for wave vectors smaller than the Thomas-Fermi wave vector. These problems (see the third column in Fig. 3) arise from the false assumption of perfect adiabatic screening in the Born-Oppenheimer approximation.

Our new method allows one to efficiently study the coupling of plasmon-phonon hybrids to electrons without the need for explicit frequency integration. Only minor modifications to the existing framework for electron-phonon coupling calculations are required. For example, the electron self-energy can be calculated as the sum over the $N_{\text{ph}} + 1$ hybrid modes, just as the sum over the phonons in electron-phonon calculations:

$$\text{Im}\Sigma_{nk}^{\text{pl-ph}} = \text{Im} \frac{1}{N_q} \sum_{m\mathbf{q}} \sum_{\beta=0}^{N_{\text{ph}}} \sum_{\pm} \frac{|\tilde{g}_{mn\beta}(\mathbf{k}, \mathbf{q})|^2 (f_{m\mathbf{k}+\mathbf{q}}^{\pm} + \tilde{n}_{\mathbf{q}\beta})}{\epsilon_{n\mathbf{k}} - \epsilon_{m\mathbf{k}+\mathbf{q}} \pm \tilde{\omega}_{\mathbf{q}\beta} + i0^+}. \quad (10)$$

Here, $\tilde{g}_{mn\beta}$ is the electron-hybrid coupling vertex [S66], N_q the number of sampled q points, $f_{m\mathbf{k}+\mathbf{q}}^+$ the Fermi-Dirac occupation at the electron energy $\epsilon_{m\mathbf{k}+\mathbf{q}}$, $f_{m\mathbf{k}+\mathbf{q}}^- = 1 - f_{m\mathbf{k}+\mathbf{q}}^+$,

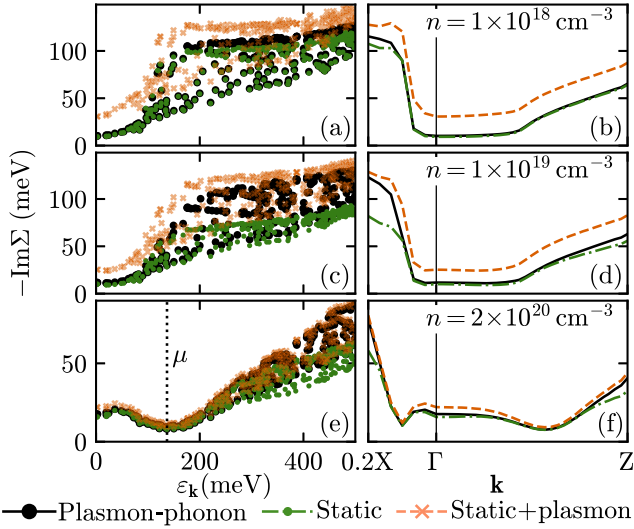


FIG. 4. (a) Imaginary electron self-energy of n -doped anatase TiO_2 at $n = 1 \times 10^{18} \text{ cm}^{-3}$ as a function of electron energy. $\varepsilon_{\mathbf{k}} = 0$ is the conduction band minimum energy. (b) The same quantity as in (a) as a function of the electron wave vector. (c)–(f) Same as in (a),(b) but for $n = 1 \times 10^{19} \text{ cm}^{-3}$ [(c),(d)] and $n = 2 \times 10^{20} \text{ cm}^{-3}$ [(e),(f)]. In (e), the vertical dotted line indicates the chemical potential μ , while in (a) and (c) μ is below the conduction band minimum.

and $\tilde{n}_{\mathbf{q}\beta} = 1/(e^{\tilde{\omega}_{\mathbf{q}\beta}/k_B T} - 1)$ the Bose-Einstein occupation of the plasmon-phonon hybrids. See Sec. S2 for details [26].

Figure 4 shows the imaginary part of the electron self-energy, which can be directly measured by angle-resolved photoemission spectroscopy [72–74]. The self-energy arising from statically screened phonons [19] can be significantly lower than the correct, hybrid-induced self-energy. A possible *ad hoc* correction is to add the bare-plasmon-induced self-energy [18,21] to the static-phonon-induced self-energy. This correction works well in the metallic regime. However, it overestimates the self-energy when the electron concentration is low because the screening of the electron-plasmon coupling by higher-energy phonons is neglected.

Our plasmon-phonon method opens the door to first-principles studies of plasmons and phonons in doped semiconductors. Because of its simplicity and efficiency, it can be widely used for many applications: various spectroscopies, optical properties, transport, and superconductivity. The calculated plasmon-phonon dispersion, spectral function, dielectric function, and electron self-energy can be directly compared with experiments such as infrared, Raman, neutron, electron energy loss, and angle-resolved photoemission spectroscopies. Formation of polaronic satellites due to plasmon-phonon hybrids [1,2,75] and superconductivity in dilute materials [76,77] are also interesting avenues for future research.

Acknowledgments—This work was supported by the Creative-Pioneering Research Program through Seoul National University, Korean NRF No. 2023R1A2C1007297, and the Institute for Basic Science (No. IBSR009-D1). Computational resources have been provided by KISTI (KSC-2022-CRE-0407).

- [1] C. Verdi, F. Caruso, and F. Giustino, Origin of the crossover from polarons to Fermi liquids in transition metal oxides, *Nat. Commun.* **8**, 15769 (2017).
- [2] J. M. Riley, F. Caruso, C. Verdi, L. Duffy, M. D. Watson, L. Bawden, K. Volckaert, G. van der Laan, T. Hesjedal, M. Hoesch *et al.*, Crossover from lattice to plasmonic polarons of a spin-polarised electron gas in ferromagnetic EuO , *Nat. Commun.* **9**, 2305 (2018).
- [3] I. Yokota, On the coupling between optical lattice vibrations and carrier plasma oscillations in polar semiconductors, *J. Phys. Soc. Jpn.* **16**, 2075 (1961).
- [4] B. B. Varga, Coupling of plasmons to polar phonons in degenerate semiconductors, *Phys. Rev.* **137**, A1896 (1965).
- [5] K. S. Singwi and M. P. Tosi, Interaction of plasmons and optical phonons in degenerate semiconductors, *Phys. Rev.* **147**, 658 (1966).
- [6] W. Cochran, R. A. Cowley, G. Dolling, and M. Elcombe, The crystal dynamics of lead telluride, *Proc. R. Soc. A* **293**, 433 (1966).
- [7] A. Mooradian and G. B. Wright, Observation of the interaction of plasmons with longitudinal optical phonons in gas, *Phys. Rev. Lett.* **16**, 999 (1966).
- [8] A. Mooradian and A. L. McWhorter, Polarization and intensity of Raman scattering from plasmons and phonons in gallium arsenide, *Phys. Rev. Lett.* **19**, 849 (1967).
- [9] A. M. Saitta, M. Lazzeri, M. Calandra, and F. Mauri, Giant nonadiabatic effects in layer metals: Raman spectra of intercalated graphite explained, *Phys. Rev. Lett.* **100**, 226401 (2008).
- [10] M. Calandra, G. Profeta, and F. Mauri, Adiabatic and nonadiabatic phonon dispersion in a Wannier function approach, *Phys. Rev. B* **82**, 165111 (2010).
- [11] D. Novko, Nonadiabatic coupling effects in MgB_2 reexamined, *Phys. Rev. B* **98**, 041112(R) (2018).
- [12] D. Novko, Broken adiabaticity induced by lifshitz transition in MoS_2 and WS_2 single layers, *Commun. Phys.* **3**, 30 (2020).
- [13] F. Giustino, Electron-phonon interactions from first principles, *Rev. Mod. Phys.* **89**, 015003 (2017).
- [14] C. Falter, M. Klenner, and W. Ludwig, Effect of charge fluctuations on the phonon dispersion and electron-phonon interaction in La_2CuO_4 , *Phys. Rev. B* **47**, 5390 (1993).
- [15] T. Bauer and C. Falter, Impact of dynamical screening on the phonon dynamics of metallic La_2CuO_4 , *Phys. Rev. B* **80**, 094525 (2009).
- [16] J. Krsnik and O. S. Barišić, Importance of coupling strength in shaping electron energy loss and phonon spectra of phonon-plasmon systems, *Phys. Rev. B* **106**, 075207 (2022).

- [17] C. S. Kengle, S. I. Rubeck, M. Rak, J. Chen, F. Hoveyda, S. Bettler, A. Husain, M. Mitrano, A. Edelman, P. Littlewood, T.-C. Chiang, F. Mahmood, and P. Abbamonte, Non-RPA behavior of the valence plasmon in $\text{SrTi}_{1-x}\text{Nb}_x\text{O}_3$, *Phys. Rev. B* **108**, 205102 (2023).
- [18] F. Caruso, C. Verdi, S. Ponc , and F. Giustino, Electron-plasmon and electron-phonon satellites in the angle-resolved photoelectron spectra of n -doped anatase TiO_2 , *Phys. Rev. B* **97**, 165113 (2018).
- [19] F. Macheda, P. Barone, and F. Mauri, Electron-phonon interaction and longitudinal-transverse phonon splitting in doped semiconductors, *Phys. Rev. Lett.* **129**, 185902 (2022).
- [20] F. Macheda, T. Sohler, P. Barone, and F. Mauri, Electron-phonon interaction and phonon frequencies in two-dimensional doped semiconductors, *Phys. Rev. B* **107**, 094308 (2023).
- [21] F. Caruso and F. Giustino, Theory of electron-plasmon coupling in semiconductors, *Phys. Rev. B* **94**, 115208 (2016).
- [22] F. Caruso, C. Verdi, and F. Giustino, Many-body calculations of plasmon and phonon satellites in angle-resolved photoelectron spectra using the cumulant expansion approach, in *Handbook of Materials Modeling: Methods: Theory and Modeling*, edited by W. Andreoni and S. Yip (Springer International Publishing, Cham, 2020), pp. 341–365.
- [23] Y. Nomura and R. Arita, *Ab initio* downfolding for electron-phonon-coupled systems: Constrained density-functional perturbation theory, *Phys. Rev. B* **92**, 245108 (2015).
- [24] J. Berges, N. Giroto, T. Wehling, N. Marzari, and S. Ponc , Phonon self-energy corrections: To screen, or not to screen, *Phys. Rev. X* **13**, 041009 (2023).
- [25] A. Marini, Equilibrium and out-of-equilibrium realistic phonon self-energy free from overscreening, *Phys. Rev. B* **107**, 024305 (2023).
- [26] See Supplemental Material at <http://link.aps.org/supplemental/10.1103/PhysRevLett.133.116402> for the derivation of the plasmon-phonon Green's function and electron-plasmon-phonon coupling and computational details, which includes Refs. [27–54].
- [27] C. Verdi and F. Giustino, Fr hlich electron-phonon vertex from first principles, *Phys. Rev. Lett.* **115**, 176401 (2015).
- [28] J. Sjakste, N. Vast, M. Calandra, and F. Mauri, Wannier interpolation of the electron-phonon matrix elements in polar semiconductors: Polar-optical coupling in GaAs, *Phys. Rev. B* **92**, 054307 (2015).
- [29] M. Royo and M. Stengel, First-principles theory of spatial dispersion: Dynamical quadrupoles and flexoelectricity, *Phys. Rev. X* **9**, 021050 (2019).
- [30] G. Brunin, H. P. C. Miranda, M. Giantomassi, M. Royo, M. Stengel, M. J. Verstraete, X. Gonze, G.-M. Rignanese, and G. Hautier, Electron-phonon beyond Fr hlich: Dynamical quadrupoles in polar and covalent solids, *Phys. Rev. Lett.* **125**, 136601 (2020).
- [31] G. Brunin, H. P. C. Miranda, M. Giantomassi, M. Royo, M. Stengel, M. J. Verstraete, X. Gonze, G.-M. Rignanese, and G. Hautier, Phonon-limited electron mobility in Si, GaAs, and GaP with exact treatment of dynamical quadrupoles, *Phys. Rev. B* **102**, 094308 (2020).
- [32] V. A. Jhalani, J.-J. Zhou, J. Park, C. E. Dreyer, and M. Bernardi, Piezoelectric electron-phonon interaction from *ab initio* dynamical quadrupoles: Impact on charge transport in wurtzite GaN, *Phys. Rev. Lett.* **125**, 136602 (2020).
- [33] J. Park, J.-J. Zhou, V. A. Jhalani, C. E. Dreyer, and M. Bernardi, Long-range quadrupole electron-phonon interaction from first principles, *Phys. Rev. B* **102**, 125203 (2020).
- [34] R. McWeeny, *Methods of Molecular Quantum Mechanics* (Academic Press, London, 1992).
- [35] R. Bauernschmitt and R. Ahlrichs, Treatment of electronic excitations within the adiabatic approximation of time dependent density functional theory, *Chem. Phys. Lett.* **256**, 454 (1996).
- [36] M. R. Filip, J. B. Haber, and J. B. Neaton, Phonon screening of excitons in semiconductors: Halide perovskites and beyond, *Phys. Rev. Lett.* **127**, 067401 (2021).
- [37] G. D. Mahan, *Many-Particle Physics*, 3rd ed. (Kluwer Academic/Plenum Publishers, New York, 2000).
- [38] G. Stefanucci and R. Van Leeuwen, *Nonequilibrium Many-Body Theory of Quantum Systems: A Modern Introduction* (Cambridge University Press, Cambridge, England, 2013).
- [39] K. S. Thygesen and A. Rubio, Nonequilibrium GW approach to quantum transport in nano-scale contacts, *J. Chem. Phys.* **126**, 091101 (2007).
- [40] H. Ness, L. K. Dash, M. Stankovski, and R. W. Godby, GW approximations and vertex corrections on the Keldysh time-loop contour: Application for model systems at equilibrium, *Phys. Rev. B* **84**, 195114 (2011).
- [41] S. Ponc , W. Li, S. Reichardt, and F. Giustino, First-principles calculations of charge carrier mobility and conductivity in bulk semiconductors and two-dimensional materials, *Rep. Prog. Phys.* **83**, 036501 (2020).
- [42] P. Giannozzi *et al.*, Advanced capabilities for materials modelling with Quantum ESPRESSO, *J. Phys. Condens. Matter* **29**, 465901 (2017).
- [43] D. R. Hamann, Optimized norm-conserving Vanderbilt pseudopotentials, *Phys. Rev. B* **88**, 085117 (2013).
- [44] M. van Setten, M. Giantomassi, E. Bousquet, M. Verstraete, D. Hamann, X. Gonze, and G.-M. Rignanese, The PseudoDojo: Training and grading a 85 element optimized norm-conserving pseudopotential table, *Comput. Phys. Commun.* **226**, 39 (2018).
- [45] J. P. Perdew and Y. Wang, Accurate and simple analytic representation of the electron-gas correlation energy, *Phys. Rev. B* **45**, 13244 (1992).
- [46] M. Horn, C. F. Schwebdtfeger, and E. P. Meagher, Refinement of the structure of anatase at several temperatures, *Z. Kristallogr.—Cryst. Mater.* **136**, 273 (1972).
- [47] G. Pizzi *et al.*, Wannier90 as a community code: New features and applications, *J. Phys. Condens. Matter* **32**, 165902 (2020).
- [48] F. Giustino, M. L. Cohen, and S. G. Louie, Electron-phonon interaction using Wannier functions, *Phys. Rev. B* **76**, 165108 (2007).
- [49] S. Ponc , E. Margine, C. Verdi, and F. Giustino, EPW: Electron-phonon coupling, transport and superconducting properties using maximally localized Wannier functions, *Comput. Phys. Commun.* **209**, 116 (2016).

- [50] N. Marzari and D. Vanderbilt, Maximally localized generalized Wannier functions for composite energy bands, *Phys. Rev. B* **56**, 12847 (1997).
- [51] N. Marzari, A. A. Mostofi, J. R. Yates, I. Souza, and D. Vanderbilt, Maximally localized Wannier functions: Theory and applications, *Rev. Mod. Phys.* **84**, 1419 (2012).
- [52] J. Bezanson, A. Edelman, S. Karpinski, and V. B. Shah, Julia: A fresh approach to numerical computing, *SIAM Rev.* **59**, 65 (2017).
- [53] S. Poncé, F. Macheda, E. R. Margine, N. Marzari, N. Bonini, and F. Giustino, First-principles predictions of Hall and drift mobilities in semiconductors, *Phys. Rev. Res.* **3**, 043022 (2021).
- [54] I. Souza, N. Marzari, and D. Vanderbilt, Maximally localized Wannier functions for entangled energy bands, *Phys. Rev. B* **65**, 035109 (2001).
- [55] Y. Liang and L. Yang, Carrier plasmon induced nonlinear band gap renormalization in two-dimensional semiconductors, *Phys. Rev. Lett.* **114**, 063001 (2015).
- [56] M. S. Hybertsen and S. G. Louie, Electron correlation in semiconductors and insulators: Band gaps and quasiparticle energies, *Phys. Rev. B* **34**, 5390 (1986).
- [57] D. A. Leon, C. Cardoso, T. Chiarotti, D. Varsano, E. Molinari, and A. Ferretti, Frequency dependence in *GW* made simple using a multipole approximation, *Phys. Rev. B* **104**, 115157 (2021).
- [58] S. Y. Savrasov, K. Haule, and G. Kotliar, Many-body electronic structure of americium metal, *Phys. Rev. Lett.* **96**, 036404 (2006).
- [59] T. Chiarotti, N. Marzari, and A. Ferretti, Unified Green's function approach for spectral and thermodynamic properties from algorithmic inversion of dynamical potentials, *Phys. Rev. Res.* **4**, 013242 (2022).
- [60] J. Bonini and J. Flick, *Ab initio* linear-response approach to vibro-polaritons in the cavity Born–Oppenheimer approximation, *J. Chem. Theory Comput.* **18**, 2764 (2022).
- [61] S. Ren, J. Bonini, M. Stengel, C. E. Dreyer, and D. Vanderbilt, Adiabatic dynamics of coupled spins and phonons in magnetic insulators, *Phys. Rev. X* **14**, 011041 (2024).
- [62] H. Toyosaki, T. Fukumura, Y. Yamada, K. Nakajima, T. Chikyow, T. Hasegawa, H. Koinuma, and M. Kawasaki, Anomalous Hall effect governed by electron doping in a room-temperature transparent ferromagnetic semiconductor, *Nat. Mater.* **3**, 221 (2004).
- [63] Y. Furubayashi, T. Hitosugi, Y. Yamamoto, K. Inaba, G. Kinoda, Y. Hirose, T. Shimada, and T. Hasegawa, A transparent metal: Nb-doped anatase TiO₂, *Appl. Phys. Lett.* **86**, 252101 (2005).
- [64] D. Kuang, J. Brilliet, P. Chen, M. Takata, S. Uchida, H. Miura, K. Sumioka, S. M. Zakeeruddin, and M. Grätzel, Application of highly ordered TiO₂ nanotube arrays in flexible dye-sensitized solar cells, *ACS Nano* **2**, 1113 (2008).
- [65] D. B. Strukov, G. S. Snider, D. R. Stewart, and R. S. Williams, The missing memristor found, *Nature (London)* **453**, 80 (2008).
- [66] O. K. Varghese, M. Paulose, and C. A. Grimes, Long vertically aligned titania nanotubes on transparent conducting oxide for highly efficient solar cells, *Nat. Nanotechnol.* **4**, 592 (2009).
- [67] F. De Angelis, C. Di Valentin, S. Fantacci, A. Vittadini, and A. Selloni, Theoretical studies on anatase and less common TiO₂ phases: Bulk, surfaces, and nanomaterials, *Chem. Rev.* **114**, 9708 (2014).
- [68] S. Moser, L. Moreschini, J. Jaćimović, O. S. Barišić, H. Berger, A. Magrez, Y. J. Chang, K. S. Kim, A. Bostwick, E. Rotenberg, L. Forró, and M. Grioni, Tunable polaronic conduction in anatase TiO₂, *Phys. Rev. Lett.* **110**, 196403 (2013).
- [69] M. Setvin, C. Franchini, X. Hao, M. Schmid, A. Janotti, M. Kaltak, C. G. Van de Walle, G. Kresse, and U. Diebold, Direct view at excess electrons in TiO₂ rutile and anatase, *Phys. Rev. Lett.* **113**, 086402 (2014).
- [70] S. Moser, L. Moreschini, J. Jaćimović, O. S. Barišić, H. Berger, A. Magrez, Y. J. Chang, K. S. Kim, A. Bostwick, E. Rotenberg, L. Forró, and M. Grioni, Tunable polaronic conduction in anatase TiO₂, *Phys. Rev. Lett.* **110**, 196403 (2013).
- [71] S. Ahn and S. Das Sarma, Theory of anisotropic plasmons, *Phys. Rev. B* **103**, L041303 (2021).
- [72] A. Bostwick, T. Ohta, T. Seyller, K. Horn, and E. Rotenberg, Quasiparticle dynamics in graphene, *Nat. Phys.* **3**, 36 (2007).
- [73] C.-H. Park, F. Giustino, M. L. Cohen, and S. G. Louie, Velocity renormalization and carrier lifetime in graphene from the electron-phonon interaction, *Phys. Rev. Lett.* **99**, 086804 (2007).
- [74] C.-H. Park, F. Giustino, C. D. Spataru, M. L. Cohen, and S. G. Louie, First-principles study of electron linewidths in graphene, *Phys. Rev. Lett.* **102**, 076803 (2009).
- [75] F. Caruso, H. Lambert, and F. Giustino, Band structures of plasmonic polarons, *Phys. Rev. Lett.* **114**, 146404 (2015).
- [76] O. Prakash, A. Kumar, A. Thamizhavel, and S. Ramakrishnan, Evidence for bulk superconductivity in pure bismuth single crystals at ambient pressure, *Science* **355**, 52 (2017).
- [77] M. N. Gastiasoro, J. Ruhman, and R. M. Fernandes, Superconductivity in dilute SrTiO₃: A review, *Ann. Phys. (Amsterdam)* **417**, 168107 (2020).